Measurement of the Canonical Equation of State of a Weakly Interacting 3D Bose Gas

C. Mordini,[1,*,†] D. Trypogeorgos,[1,2,†] A. Farolfi,[1,2] L. Wolswijk,[1,2] S. Stringari,[1] G. Lamporesi,[1,2] and G. Ferrari[1,2]

[1]*INO-CNR BEC Center and Dipartimento di Fisica, Università di Trento, Povo 38123, Italy*[‡]

[2]*Trento Institute for Fundamental Physics and Applications, INFN, Povo 38123, Italy*

(Received 30 March 2020; accepted 8 September 2020; published 9 October 2020)

Using a multiple-image reconstruction method applied to a harmonically trapped Bose gas, we determine the equation of state of uniform matter across the critical transition point, within the local density approximation. Our experimental results provide the canonical description of pressure as a function of the specific volume, emphasizing the dramatic deviations from the ideal Bose gas behavior caused by interactions. They also provide clear evidence for the nonmonotonic behavior with temperature of the chemical potential, which is a consequence of superfluidity and Bose-Einstein condensation. The measured thermodynamic quantities are compared to mean-field predictions available for the interacting Bose gas. The limits of applicability of the local density approximation near the critical point are also discussed, focusing on the behavior of the isothermal compressibility.

DOI: 10.1103/PhysRevLett.125.150404

Introduction.—Although 25 years have passed since the first realization of a Bose-Einstein condensate (BEC) in a dilute gas of alkali atoms, the experimental investigation of the equation of state (EOS) of a weakly interacting Bose gas is still rather incomplete. The EOS of the ideal Bose gas (IBG) predicts peculiar features at finite temperature, e.g., saturation of the thermal component and infinite compressibility in the BEC phase, so it is of major importance to have a direct experimental access to the crucial role of interactions which violate the IBG behavior. Experiments at finite temperature have focused on the role of interactions on the temperature dependence of the BEC fraction [1,2] and on the value of the critical temperature in both harmonically trapped and uniform configurations [3,4]. Results on the EOS of both 3D [5,6] and 2D [7,8] Bose gases have been obtained in the framework of the grand canonical approach, where the pressure of the uniform gas is expressed in terms of the chemical potential. At zero temperature the above approach has proven successful in identifying the Lee-Huang-Yang correction to the EOS originating from beyond-mean-field quantum fluctuations [9].

Atomic samples trapped by nonuniform potentials can be used to extract the thermodynamic behavior of uniform matter through the use of the local density approximation (LDA) [10,11]. In 3D, the pressure is extracted from the measured column density of the trapped gas using the Gibbs-Duhem relation, while the chemical potential is usually obtained fitting the density distribution of the sample, with the exception of the unitary Fermi gas where the model-dependent measurement of the chemical potential was successfully avoided by measuring the compressibility of the gas [12].

In this Letter, we obtain the EOS of a uniform, 3D, weakly interacting Bose gas at constant temperature T using the LDA method. We measure the density profile of a trapped atomic sample exploiting the axial symmetry of the trapping potential through the inverse Abel transform [13]. This provides direct access to the canonical formulation of the EOS.

The canonical and grand canonical descriptions are in principle equivalent in the thermodynamic limit: the density of the system, which is the key variable of the canonical picture, can be derived starting from measurements of grand canonical variables with the use of fundamental thermodynamic relations. Experimentally, however, this procedure is technically demanding in 3D Bose gases and has never been realized so far. Here we circumvent this through a direct measurement of the density of the trapped gas. This allows us to explore important features of the system evident in the canonical formulation, like the behavior of the pressure $p(v, T)$ at fixed temperature T as a function of the specific volume $v = 1/n$, and the nonmonotonic behavior of the chemical potential μ as a function of the reduced temperature T/T_c [14]. We note that the thermodynamics of the 3D Bose gas is not universal, but it depends on the specific strength of atomic interactions fixed by the scattering length a. Here we investigate the behavior of the EOS as a function of the density n, at constant a and T.

The density of a 3D condensed gas spans several orders of magnitude from the visible thermal tails to the dense condensate center, requiring an imaging method with a much higher dynamic range than usual absorption imaging. We tackle this using partial-transfer absorption

imaging (PTAI) [15,16] and a reconstruction method that produces highly accurate spatial profiles even for very dense samples [17].

Experimental procedure.—We produce partially condensed ^{23}Na gases confined in a Ioffe-Pritchard trap with axial (radial) trapping frequency $\omega_x/2\pi = 8.83(2)$ Hz [$\omega_\rho/2\pi = 100.8(7)$ Hz], where we let the BEC equilibrate for 2s after the end of the evaporation ramp. We then extract a few percent of the atoms and image them *in situ* along the vertical direction z, obtaining an image of a tunable fraction of the column density $n_1(x,y) = \int n dz$. We implement PTAI by radiating the sample with microwaves of Rabi frequency $\Omega/2\pi = 60.7(2)$ kHz to out-couple a fraction of the atoms from $|F, m_F\rangle = |1,-1\rangle$, where they are magnetically trapped, to $|2,-2\rangle$ in the upper hyperfine manifold. The extracted atoms are subsequently imaged with π-polarized light resonant with the $F = 2 \to F' = 3$ cycling transition using a 5-μs-long probe pulse with $I/I_{\rm sat} = 4$, where $I_{\rm sat}$ is the saturation intensity of ^{23}Na [18]. This process takes only a few microseconds and so it does not suffer from any losses due to spin flipping collisions, which are further suppressed by conservation of angular momentum. We then release the remaining atoms from the trap and image them along y after a time of flight of 50 ms. Imaging at high intensity allows us to calibrate the absorption cross section, obtaining an absolute measure of the atomic density [19]. Details on the imaging calibration are provided in the Supplemental Material [20].

The reconstruction method combines multiple partial-transfer images to obtain a high-dynamic-range image of the column density. *In situ* measurements of n_1 are done for several microwave pulse times τ extracting a fraction $\sin^2(\Omega\tau/2)$ of the atomic sample each time. Long pulses, between 1.5 to 2.5 μs (extracting 8% to 20%), yield a saturated image of the condensed part but allow to image the thermal tails with high signal-to-noise ratio. Short pulses, of 0.5 to 1.5 μs (1% to 8%), lead to an accurate image of the denser BEC core but the thermal tails are no longer visible. In both cases the spectrum of the microwave pulse is broad enough to neglect the spatial detuning due to the trapping magnetic field and to consider extractions as uniform. We crop each image at a threshold set by the imaging conditions to retain only the nonsaturated region, rescale it by the extraction fraction, and finally average all of them. In the Supplemental Material [20] we discuss in details the microwave extraction procedure and the choice of the threshold for the reconstruction method. From the reconstructed n_1 [Fig. 1(a)] we obtain the pressure and density along the long axis x of the sample. We independently measure the temperature from the time-of-flight image by fitting the wings of the thermal distribution to a Bose function, taking into account effects due to the nonballistic expansion from our elongated trap [25].

The pressure of the gas along x is $p = m\omega_\rho^2/2\pi \int n_1 dy$, where m is the atomic mass. It is obtained integrating the

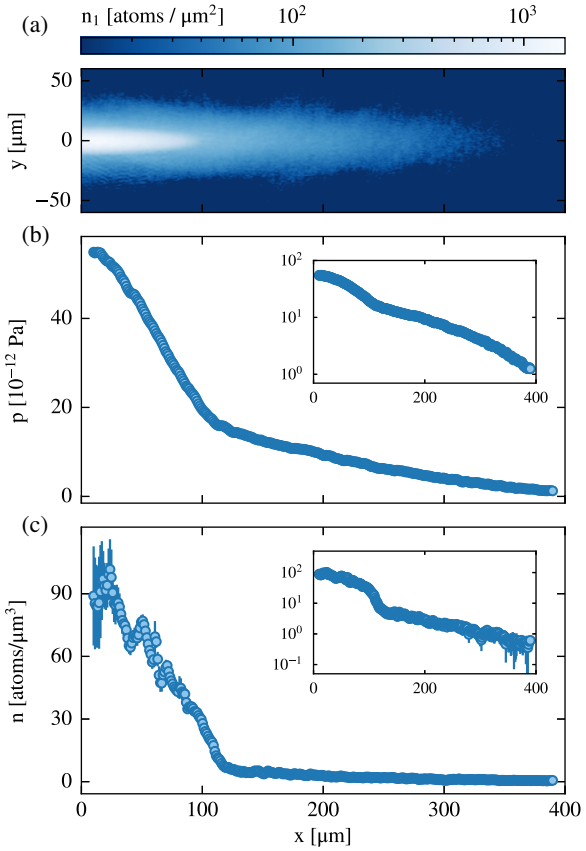

FIG. 1. (a) Column density of the trapped sample, reconstructed from different partial extractions. Each pixel in the image results from the average of 5 to 80 images at different extraction ratios. (b) Pressure along the x axis of the sample, obtained integrating n_1 along y. The error bars on the pressure are smaller than the marker size. (c) Axial density profile of the sample $n(x)$ obtained via the inverse Abel transform. The insets in (b) and (c) show pressure and density of the gas in log scale, highlighting the high dynamic range needed to capture the different regimes of the Bose gas thermodynamics.

Gibbs-Duhem relation $dp = nd\mu + sdT$ at constant temperature, where s is the entropy density, and assuming the LDA relation $\mu = \mu_0 - V_{\rm ext}$, where $V_{\rm ext}$ is the trapping potential and μ_0 is the value of the chemical potential in the trap center [10,11]. The *in situ* density can be calculated either from the Gibbs-Duhem relation $n = (\partial p/\partial\mu)_T = -(\partial p/\partial V_{\rm ext})_T$ or from the inverse Abel transform. In Section IV of the Supplemental Material [20], we provide an explicit comparison between the two methods. Using the Abel transform, we obtain a 2D slice $n(x,y)$ of the density along the imaging plane, that we azimuthally average to obtain a low-noise profile of the density along the x axis. Figures 1(b) and 1(c) show the pressure and density along x for a sample of $5.4(5) \times 10^6$ atoms with a temperature $T = 280(10)$ nK, corresponding to a BEC fraction of about 50% with a sizable thermal component. The error bars in this and in the following figures are due to the uncorrelated combination of statistical and systematic errors on the

reconstructed column density, of which we give a detailed description in [20].

Our configuration is well suited to explore the thermodynamics of the uniform gas in a wide range of densities, that we map to the reduced temperature T/T_c, where $T_c = (2\pi\hbar^2/mk_B)(n/\zeta_{3/2})^{2/3}$ is the local critical temperature. Here ζ_ν is the Riemann zeta function evaluated at ν. At the trap center, where the density is maximum, we have $T/T_c \sim 0.2$, while in the thermal tails it rapidly becomes larger than 1. From the peak density we evaluate the gas parameter $na^3 = 2 \times 10^{-6}$. Since $na^3 \ll 1$, the deviations from the predictions of mean field theory are expected to be small, except close to the critical point, as opposed to the ones from IBG that largely fail below the critical point.

Canonical EOS $p(v)$ and compressibility.—Figure 2(a) shows the measurement of the canonical EOS $p(v)$ at constant temperature in reduced variables, rescaled by the relevant critical quantities at the verge of condensation, $p_c = \zeta_{5/2}k_BT/\lambda_T^3$ and $v_c = 1/n_c = \lambda_T^3/\zeta_{3/2}$, where $\lambda_T = (2\pi\hbar^2/mk_BT)^{1/2}$ is the thermal wavelength. The specific volume is related to the local critical temperature by $v/v_c = (T/T_c)^{3/2}$.

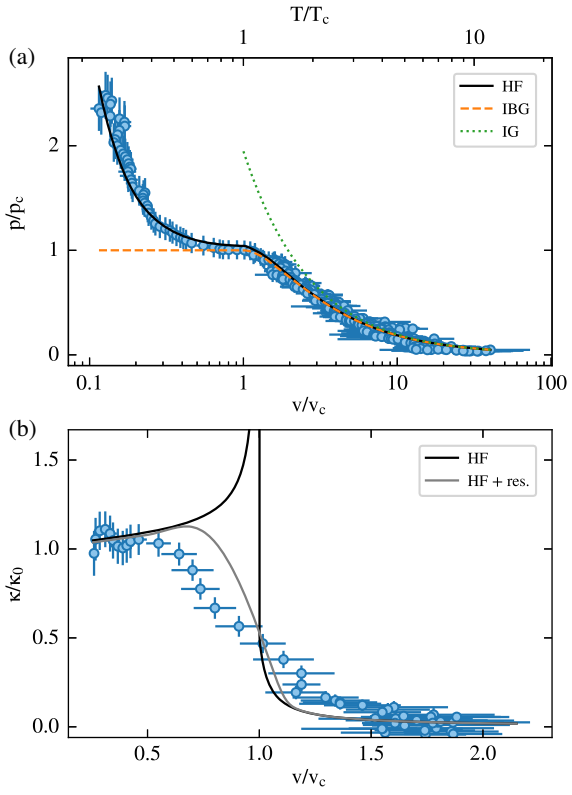

FIG. 2. (a) Measurement of the canonical EOS of a uniform Bose gas, showing the pressure as a function of the specific volume at constant $T = 280$ nK. Pressure and density are derived within the LDA from the *in situ* distribution of a harmonically trapped sample. The HF prediction (solid) for a uniform system at the same temperature shows good agreement in the whole range without fitting parameters. Predictions from the IG (dotted) and IBG (dashed) models are shown for comparison. (b) Experimental results for the reduced compressibility versus v/v_c compared to HF theory, which predicts a narrow peak at the critical point. The gray solid line includes the effects of the finite imaging resolution applied to a numerical simulation of the HF density profile in our trap.

The experimental results in Fig. 2(a) are compared to the Hartree-Fock (HF) EOS for uniform matter. The model considers an interacting gas with the following densities for the condensate and thermal fractions, respectively

$$n_0 = \mu/g - 2n_T,$$
$$n_T = \frac{1}{\lambda_T^3} g_{3/2}(e^{(\mu-2gn)/k_BT}), \tag{1}$$

where $g = 4\pi\hbar^2 a/m$, and g_ν is the polylogarithm function of index ν. The pressure

$$p = gn^2 - \frac{1}{2}gn_0^2 + \frac{k_BT}{\lambda_T^3} g_{5/2}(e^{(\mu-2gn)/k_BT}) \tag{2}$$

can be directly derived from Eqs. (1). The black line in Fig. 2(a) shows the HF EOS evaluated at the experimental value $T = 280$ nK, without fitting parameters. We find good agreement between experiment and HF prediction, confirming the validity of the mean field approach for the description of a weakly interacting gas. For $v/v_c > 1$, the pressure corresponds to that of an ideal (noninteracting) Bose gas (IBG). In the same figure we also show the prediction of the classical ideal gas law $p = k_BT/v$ (IG), which correctly captures the behavior of p only for large v/v_c, revealing the importance of quantum effects in the vicinity of the critical point. In the region $v/v_c < 1$, the strong increase in the pressure, which diverges as $(\zeta_{3/2}^2/\zeta_{5/2})(a/\lambda_T)(v_c/v)^2$, shows that the thermodynamics is largely dominated by the effect of the interactions. The explicit dependence on a/λ_T reveals the nonuniversality of the EOS.

Next, we discuss the isothermal compressibility of the gas defined as $\kappa = (1/n)\partial n/\partial p|_T$. Figure 2(b) shows our measurement of κ, normalized by the $T = 0$ value $\kappa_0 = 1/gn^2$, as a function of the reduced specific volume. The experimental results quantitatively agree with the HF prediction (black line) at small v/v_c and show a rapid transition across the critical point. They however strongly deviate from the mean-field prediction in the critical region.

The disagreement can have different origins. (i) The mean field HF theory does not account for the large fluctuation effects characterizing the critical region, which, according to Ginzburg-Landau arguments, corresponds to the range $|\mu - \mu_c| \sim m^3g^2k_B^2T_c^2/\hbar^6$, with μ_c as the chemical potential evaluated at the transition [26,27], i.e., to the temperature interval $\Delta T/T \sim an^{1/3}$. At the transition $n \sim n_c$ and we have $an_c^{1/3} = (\zeta_{3/2})^{1/3}a/\lambda_T \sim 5 \times 10^{-3}$. The dependence on a/λ_T signals again a violation of universality. (ii) The HF curve is based on the

corresponding theory for uniform matter, and does not account for the corrections to the LDA which take place near the transition between the BEC and the normal phase in a trapped system. These lead to a finite thickness of the boundary of the condensate, scaling with the Thomas-Fermi radius R_x as $d = (a_x^4/2R_x)^{1/3}$ [28]. This is a finite-size effect, since R_x depends on the number of atoms in the condensate. We also expect that this result is only weakly affected by the presence of a thermal component. Along the weak axis of our trap $R_x \sim 100$ μm and we have $d \sim 2$ μm. (iii) Finally, the finite resolution of the imaging system (~ 2 μm) smears the sharp features in the density profile. The gray curve in Fig. 2(b) shows κ resulting from a numerical simulation of the column density predicted by HF theory within LDA, and convoluted with our experimental imaging resolution. The remaining differences with respect to the experimental curve are then likely due to the failure of HF theory near the transition and to the violation of the LDA. These are stringent limitations for the measurement of the compressibility in weakly interacting Bose gases as compared to the unitary Fermi gas, where the width of the critical region is much larger as the only energy scale at unitarity is fixed by the Fermi energy, and experiments revealed the occurrence of a peak in κ.

Chemical potential $\mu(T)$.—The chemical potential plays a crucial role in the physics of Bose-Einstein condensed gases and it is consequently important to understand its behavior at finite temperature. A peculiar feature concerns its nonmonotonic dependence across the critical region. Below the critical point, two effects are responsible for the monotonic increase of $\mu(T)$. At low temperatures ($T < gn/k_B$) it is a consequence of the thermal excitation of phonons, determining $\mu \sim T^4$. At higher temperatures it increases like $T^{3/2}$ as a consequence of the exchange effects characterizing the thermal contribution to the energy of the system [29] (see also Section VI of [20]). Above the critical point, it instead starts decreasing and eventually reaches the typical decay $k_B T \ln(n\lambda_T^3)$ exhibited by classical gases. HF theory captures the presence of exchange effects, where the ratio μ/gn, equal to 1 at $T = 0$, reaches a peak value of 2 at the transition, where $n_T = n$ [see Eq. (1)]. The nonmonotonic behavior of the chemical potential is not a peculiarity of dilute Bose gases, but characterizes in general the thermodynamic behavior of neutral superfluids. This feature, already observed in the unitary Fermi superfluid gas [12] and confirmed by the thermodynamic behavior of liquid ^{4}He, has not been so far measured in bosonic ultracold gases.

Within the LDA, the knowledge of $V_{\rm ext}$ is sufficient to measure the chemical potential up to the constant μ_0. We have determined the value $\mu_0/k_B = 66.7(2)$ nK fitting the density to the HF profile calculated at $T = 280$ nK. The result for μ/gn as a function of T/T_c is shown in Fig. 3, clearly revealing its nonmonotonic behavior with a peak around $T = T_c$. In the LDA-based scheme, T/T_c is scanned at fixed T by the spatial variation of T_c, which depends on the density. The relevant range across the transition point, $0.2 \leq T/T_c \leq 1.5$, corresponds to the spatial region 10 μm $\leq x \leq 150$ μm.

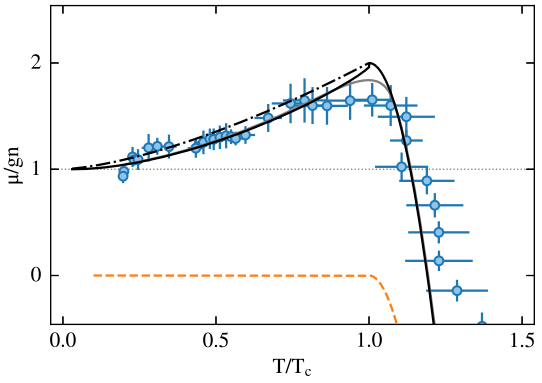

FIG. 3. Grand canonical EOS for an interacting Bose gas at constant temperature $T = 280$ nK. The chemical potential, in units of the local interaction term gn, goes from 1 to 2 as the reduced temperature T/T_c goes from 0 to the critical point, and decreases in the thermal region ($T/T_c > 1$). Black solid and dot-dashed lines show the HF and $1 + (T/T_c)^{3/2}$ predictions, respectively, while the gray solid line includes the effects of the finite imaging resolution applied to a numerical simulation of the HF density profile in our trap. The dashed line is the IBG law.

The discrepancy in the vicinity of the transition is due to the same reasons examined in the analysis of the compressibility. We see that those limitations have a much smaller effect on the determination of $\mu(T)$ compared to Fig. 2(b), where the dependency on the strong density gradient is more affected by the approximations discussed above. The dot-dashed line in Fig. 3 shows the universal curve $\mu/gn = 1 + (T/T_c)^{3/2}$, corresponding to the lowest order approximation for μ in terms of g, obtained by using the IBG result for the thermal fraction n_T. Higher-order corrections to this law stem from the non universality of the Bose gas EOS and affect the exact shape of the curve, but not its non-monotonicity. In Section VI of the Supplemental Material [20], we present the measurement of the same EOS on an atomic sample at a lower temperature, where the determination of μ_0 does not require the comparison with the HF calculation of the density profile, and find comparable results. More precise and systematic measurements of the temperature dependence of the chemical potential might provide quantitative estimates of the deviations of μ/gn from the law $1 + (T/T_c)^{3/2}$, caused by the inclusion of beyond mean field effects [30].

Grand canonical EOS $p(\mu)$.—The above results can be also discussed in the framework of the grand canonical ensemble, where μ is the independent thermodynamic variable. In [5] it was shown that the dependence of the pressure on the inverse fugacity $\zeta = e^{-\mu/k_B T}$ reveals a typical cusp behavior at the transition point, with a critical value $\zeta_c \sim 1$, which however could not be measured with

sufficient precision to reveal the presence of interaction effects at the transition. Our analysis shows a critical value of $\zeta_c < 1$, corresponding to a positive shift in the chemical potential in agreement with the results of Fig. 3. The results for the reduced pressure p/p_c as a function of the inverse fugacity are reported and discussed in detail in [20].

In conclusion, this work contributes to the study of the thermodynamics of a 3D weakly interacting bosonic gas. For the first time we obtain the EOS in the canonical formulation $p(v)$, and highlight the fundamental role of interactions in the finite temperature behavior of a Bose gas. We provide evidence for the nonmonotonic temperature dependence of the chemical potential across the phase transition, a fundamental property which has not been observed before in a weakly interacting superfluid. Our measurements were possible thanks to the development of an accurate, high-dynamic-range novel imaging method [17]. This approach can be readily applied to other trapped degenerate quantum systems, including the novel phases of interacting quantum mixtures. Our results lay the groundwork for further investigation of the EOS around the critical region.

We are grateful to M. Ota, S. Giorgini, L. Pitaevskii, and C. Salomon for fruitful discussions, and M. Tharrault for contributions at the early stages of this project. We thank the whole BEC Center and the Q@TN initiative. We acknowledge funding from the project NAQUAS of QuantERA ERA-NET Cofund in Quantum Technologies (Grant Agreement No. 731473) implemented within the European Unions Horizon 2020 Programme, and from Provincia Autonoma di Trento.

*carmelo.mordini@unitn.it
†These two authors contributed equally.
‡http://bec.science.unitn.it.

[1] R. P. Smith, R. L. D. Campbell, N. Tammuz, and Z. Hadzibabic, Phys. Rev. Lett. **106**, 250403 (2011).
[2] N. Tammuz, R. P. Smith, R. L. D. Campbell, S. Beattie, S. Moulder, J. Dalibard, and Z. Hadzibabic, Phys. Rev. Lett. **106**, 230401 (2011).
[3] F. Gerbier, J. H. Thywissen, S. Richard, M. Hugbart, P. Bouyer, and A. Aspect, Phys. Rev. A **70**, 013607 (2004).
[4] I. Gotlibovych, T. F. Schmidutz, A. L. Gaunt, N. Navon, R. P. Smith, and Z. Hadzibabic, Phys. Rev. A **89**, 061604(R) (2014).
[5] S. Nascimbène, N. Navon, F. Chevy, and C. Salomon, New J. Phys. **12**, 103026 (2010).
[6] R. Meppelink, R. A. Rozendaal, S. B. Koller, J. M. Vogels, and P. van der Straten, Phys. Rev. A **81**, 053632 (2010).
[7] T. Yefsah, R. Desbuquois, L. Chomaz, K. J. Günter, and J. Dalibard, Phys. Rev. Lett. **107**, 130401 (2011).
[8] R. Desbuquois, T. Yefsah, L. Chomaz, C. Weitenberg, L. Corman, S. Nascimbène, and J. Dalibard, Phys. Rev. Lett. **113**, 020404 (2014).
[9] N. Navon, S. Piatecki, K. Günter, B. Rem, T. C. Nguyen, F. Chevy, W. Krauth, and C. Salomon, Phys. Rev. Lett. **107**, 135301 (2011).
[10] C.-H. Cheng and S.-K. Yip, Phys. Rev. B **75**, 014526 (2007).
[11] T.-L. Ho and Q. Zhou, Nat. Phys. **6**, 131 (2010).
[12] M. J. H. Ku, A. T. Sommer, L. W. Cheuk, and M. W. Zwierlein, Science **335**, 563 (2012).
[13] Y. Shin, M. W. Zwierlein, C. H. Schunck, A. Schirotzek, and W. Ketterle, Phys. Rev. Lett. **97**, 030401 (2006).
[14] D. J. Papoular, G. Ferrari, L. P. Pitaevskii, and S. Stringari, Phys. Rev. Lett. **109**, 084501 (2012).
[15] D. V. Freilich, D. M. Bianchi, A. M. Kaufman, T. K. Langin, and D. S. Hall, Science **329**, 1182 (2010).
[16] A. Ramanathan, S. R. Muniz, K. C. Wright, R. P. Anderson, W. D. Phillips, K. Helmerson, and G. K. Campbell, Rev. Sci. Instrum. **83**, 083119 (2012).
[17] C. Mordini, D. Trypogeorgos, L. Wolswijk, G. Lamporesi, and G. Ferrari, Opt. Express **28**, 29408 (2020).
[18] M. Horikoshi, A. Ito, T. Ikemachi, Y. Aratake, M. Kuwata-Gonokami, and M. Koashi, J. Phys. Soc. Japan **86**, 104301 (2017).
[19] G. Reinaudi, T. Lahaye, Z. Wang, and D. Guéry-Odelin, Opt. Lett. **32**, 3143 (2007).
[20] See the Supplemental Material at http://link.aps.org/supplemental/10.1103/PhysRevLett.125.150404 for details on the calibration of experimental parameters, the error budget, and further discussion on theory details, which includes Refs. [21–24].
[21] J. Dalibard and C. Cohen-Tannoudji, J. Phys. B **18**, 1661 (1985).
[22] P. Holoborodko, Smooth noise robust differentiators (2008), http://www.holoborodko.com/pavel/numerical-methods/numerical-derivative/smooth-low-noise-differentiators/.
[23] E. W. Hansen and P.-L. Law, J. Opt. Soc. Am. A **2**, 510 (1985).
[24] S. Gibson, D. D. Hickstein, R. Yurchak, M. Ryazanov, D. Das, and G. Shih, Pyabel/pyabel: v0.8.3 (2019), https://doi.org/10.5281/zenodo.3370021.
[25] J. Szczepkowski, R. Gartman, M. Witkowski, L. Tracewski, M. Zawada, and W. Gawlik, Rev. Sci. Instrum. **80**, 053103 (2009).
[26] S. Giorgini, L. P. Pitaevskii, and S. Stringari, Phys. Rev. A **54**, R4633 (1996).
[27] P. Arnold and B. Tomášik, Phys. Rev. A **64**, 053609 (2001).
[28] F. Dalfovo, L. P. Pitaevskii, and S. Stringari, Phys. Rev. A **54**, 4213 (1996).
[29] L. Pitaevskii and S. Stringari, *Bose-Einstein Condensation and Superfluidity* (Oxford University Press, New York, 2016), https://dx.doi.org/10.1093/acprof:oso/9780198758884.001.0001.
[30] A discussion of the mean-field and beyond-mean-field predictions for the temperature dependence of the chemical potential in a dilute Bose gas, including a comparison with numerical Monte Carlo simulations, is reported in M. Ota and S. Giorgini, arXiv:2008.05246.